Oxid Met (2015) 83:1–27
DOI 10.1007/s11085-014-9506-3

ORIGINAL PAPER

KCl-Induced Corrosion of the FeCrAl Alloy Kanthal® AF at 600 °C and the Effect of H_2O

N. Israelsson · K. Hellström · J.-E. Svensson · L.-G. Johansson

Received: 30 May 2013 / Revised: 17 October 2014 / Published online: 29 October 2014

Abstract The present study investigates the influence of H_2O and KCl on the high-temperature corrosion of the FeCrAl alloy Kanthal® AF. Polished samples, with and without applied KCl, were exposed isothermally to O_2 or $O_2 + H_2O$ at 600 °C. The samples were investigated using TGA, XRD, SEM/EDX, AES and IC. It was found that KCl accelerates corrosion and that a rapidly growing iron, chromium-rich oxide forms in both environments. Chromate formation and alloy chlorination are shown to initiate the formation of non-protective oxide scales. In addition, aluminium nitrides form in the alloy substrate in both environments.

Keywords FeCrAl · High temperature corrosion · Water vapour · KCl

Introduction

It is well known that the high-temperature corrosion of chromia-forming steels in an oxidising environment is accelerated by alkali chlorides and by high concentrations of water vapour [1–14]. The accelerated effect of water vapour has been shown to be connected to chromia evaporation in the form of $CrO_2(OH)_2$ [1, 2]. The resulting chromium-depleted $(Fe,Cr)_2O_3$ mixture has poor protective properties in comparison to the chromium-rich mixed oxide. This corrosion mechanism of stainless steel is significant at temperatures as low as 600 °C.

The high corrosivity of alkali chlorides on stainless steel at elevated temperatures has been attributed to an "active corrosion" (chlorine cycle) mechanism [3–5, 9–12],

N. Israelsson (✉) · K. Hellström · J.-E. Svensson · L.-G. Johansson
The Swedish Competence Centre for High Temperature Corrosion, Department of Environmental Inorganic Chemistry, Chalmers University of Technology, SE-412 96 Göteborg, Sweden
e-mail: niklas.israelsson@chalmers.se

where alkali chlorides primarily are regarded as sources for molecular chlorine. However, recent reports show that the alkali cation also plays an important role in the corrosion attack [6, 7, 15]. Initially, alkali reacts with chromia in the protective oxide to form a solid alkali chromate (VI). The reactions are rapid at 600 °C and also result in the conversion of the protective oxide into a poorly protective iron-rich scale. Subsequently, chlorine or chloride ions can penetrate the scale, forming transition metal chlorides at the scale metal interface. The formation of sub-scale chlorides further accelerates corrosion due, for example, to decreased scale adhesion.

In contrast to chromia (and the solid-solution $(Cr_xFe_{1-x})_2O_3$), alumina (Al_2O_3) is not expected to form compounds with alkali chlorides at intermediate temperature. Consequently, it appears worthwhile to investigate the usefulness of alumina-forming alloys (e.g., FeCrAl) in environments where chromia-forming stainless steels suffer from rapid corrosion. The literature on the corrosion properties of FeCrAl alloys at temperatures lower than 700 °C is quite scarce, however some studies have been performed [13, 16, 17]. The common view is that the temperature is too low to obtain a protective oxide scale on FeCrAl alloys. This work addresses the corrosion behaviour of an FeCrAl alloy (Kanthal® AF) in the presence of KCl in dry and wet environments.

Experimental Methods

Material and Preparation

A commercial FeCrAl alloy, Kanthal® AF containing nominally 21 wt% Cr, 5 wt% Al balanced with Fe (for nominal composition, see Table 1) was used in this study. In addition to the main alloying elements, very small amounts of trace elements (Si, Mn and Mg) and reactive elements (Y, Zr) were present in the alloy. A detailed description of the oxidation behaviour of the reactive elements can be found in Ref. [18]. The samples were ground and polished down to 1 μm finish, thereafter they were ultrasonically cleaned in water, acetone and ethanol. A saturated solution of KCl in water/ethanol was used for applying KCl to the surfaces. The specimen was alternately sprayed and dried with warm air (~35 °C) in order to avoid the formation of droplets on the surface. Each sample was applied with 0.05 mg KCl/cm^2. The samples were then placed in a desiccator to cool, and their weight was recorded using an analytical balance. The size of the salt crystals was in the range of 10–50 μm, see Fig. 1. The corrosion exposure was started immediately after recording the sample mass.

Exposures

The exposures were performed in a horizontal tube furnace and a Setaram instrument with 5 % O_2 + 95 % N_2 or 5 % O_2 + 40 % H_2O + 55 % N_2 at 600 °C. The flow rate in the tube furnace was 1,000 ml/min, which corresponds to 3.2 cm/s,

Table 1 Nominal chemical composition of Kanthal® AF

Element	Cr	Al	Mn	Si	C	Fe	RE
wt%	20.5–23.5	5.3	0.4	0.7	0.08	bal.	Y, Zr

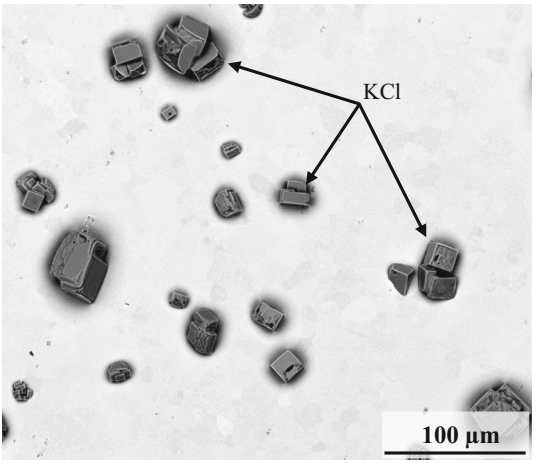

Fig. 1 SEM-BSE image of unexposed Kanthal® AF with KCl applied to the surface

and the exposure times were 1, 24, 72 and 168 h. The TGA measurements were performed up to 72 h with a flow rate of 15 ml/min, which corresponds to 0.3 cm/s. Humidification was achieved by saturating the exposure gas with water vapour at the desired dew point (76.4 °C), equivalent to 40 vol% water vapour. The samples were mounted on an alumina holder and introduced to the tube furnace or hung in the Setaram system. After exposure the samples were allowed to cool in dry air in a desiccator. Reference exposures were performed for 168 h in both dry and humid atmosphere in the absence of KCl.

Analytical Techniques

X-Ray Diffraction, XRD

A Siemens D5000 powder diffractometer was used to determine the crystalline corrosion products. The instrument was equipped with a grazing-incidence-beam attachment together with a Göbel mirror. The samples were exposed to a source of CuK_{α} radiation ($\lambda = 1.5418$ Å) with an incident angle of 0.5°–1.5°. The moving detector collected data in the range of $20° < 2\theta < 65°$ with step size of 0.05°. Silicon powder was added to the sample surfaces for calibration. The background was subtracted from the diffraction measurements.

Thermo Gravimetric Analysis, TGA

A Setaram TAG thermobalance was used to study the oxidation kinetics at 600 °C for up to 72 h. An alumina reference sample with the same geometry as the exposed sample was used to diminish the buoyancy effect. In addition, the ex situ weight gains were recorded using an analytical balance. The data were plotted from the time when the isothermal exposure temperature was reached. The time to reach 600 °C was about 6 min.

Ion Chromatography, IC

A Dionex ICS-90 system was used to establish the amount of water-soluble anions (CrO_4^{2-}, Cl^-) on the surface after exposure. The anions were analysed with an IonPac AS4A-SC analytic column and with 1.8 mM Na_2CO_3/1.7 mM $NaHCO_3$ as elution. A Dionex OnGuard II H was used to prevent metal ions from entering the column. The samples were leached in 5 ml Milli-Q water using ultrasonic agitation for 10 + 10 min. The elution was 20 mM sulfonic acid and the flow rate was 2 ml/min. The detection limits for the different species were: $Cl^- = 0.03$ and $CrO_4^{2-} = 0.01$ μmol.

Scanning Electron Microscopy with Energy Dispersive X-ray Spectroscopy, SEM/EDX

The microscopy analysis was done using an FEI Quanta 200 FEG ESEM operated in high vacuum mode. The instrument was equipped with an Oxford Inca EDX system, which was used for chemical quantification and elemental mapping. The ESEM was operated at 8–10 kV for imaging and EDX analysis.

A Gatan Ilion+ broad ion beam system was used to prepare cross sections by sputtering argon ions. The ion gun was operated at 6 kV and the sputter time was 2–3 h.

Auger Electron Spectroscopy, AES

Auger electron spectroscopy was used to estimate oxide thickness and to determine elemental depth distribution. The AES analyses were performed with a PHI 660 scanning auger microprobe (SAM) using an accelerating voltage of 10 kV and a beam current of 200 nA. AES depth profiling was performed using ion sputtering with 3.5 keV Ar+. Two areas were analysed; one smaller 10×10 μm^2 and one larger 90×120 μm^2. They exhibited almost the same oxide thickness and elemental depth distribution.

Quantitative analyses were performed using the peak-to-peak height of the Auger transitions of a specific element together with sensitivity factors provided by PHI, except for the Al and O, which were calibrated against pure Al_2O_3. Since the sensitivity factors for oxygen in Cr_2O_3 and Fe_2O_3 are different from that for Al_2O_3 the oxygen signal will be slightly off when mixtures of the oxides are present [19].

The computer software PHI-Matlab and linear least square (LLS) routines were used to separate the oxide and metal components in the depth profiles.

Results

Oxidation in Dry O_2 and $O_2 + H_2O$

Exposure of Kanthal® AF for 168 h in O_2 and $O_2 + H_2O$ at 600 °C in the absence of KCl resulted in very low mass gains, about 7 μg/cm^2 in dry O_2 and 9 μg/cm^2 in $O_2 + H_2O$. After exposure, the surface was almost featureless, being covered by a thin and smooth oxide film. In addition, RE-rich oxide particles (1–3 μm in diameter) were scattered over the surface. After 168 h exposure the oxide film was analysed using AES, showing a thickness of the base oxide of about 45 nm in O_2 (not shown) and 55 nm in $O_2 + H_2O$ (Fig. 2), in good agreement with the recorded mass gains. The analyses showed essentially the same oxide composition in the two environments. The oxide film was dominated by aluminium but significant amounts of iron and chromium were also present. Chromia was enriched in a band in the middle of the oxide film while iron oxide was consistently found outside the chromia band. The bottom part of the film consisted of relatively pure aluminium oxide. Thus the oxide film was dominated by aluminium (30–40 at.% Al) and also contained 0–10 at.% of Fe and Cr. XRD showed clear evidence of chromium-rich corundum-type Me_2O_3 while no aluminium-containing crystalline product was identified. The film formed after 24 h (not shown) was similar to the one formed after 168 h, except that it was slightly thinner and less aluminium-rich.

Oxidation in Dry O_2 in the Presence of KCl

Gravimetry

Figure 3 shows mass gain in O_2 at 600 °C in the presence of KCl. After 72 h, the mass gain was about 40 times higher than the samples exposed in the absence of KCl (not shown). The mass gains were large compared to the amount of KCl added before exposure (0.05 mg/cm^2). The mass gain was relatively rapid during the first 24 h and then continued at a slower rate. The samples subjected to 168 h of exposure in the tube furnace exhibited breakaway corrosion and scale spallation during cooling. The in situ TG curves in Fig. 4 provide much more detail on the reaction kinetics than Fig. 3. They are described in the $O_2 + H_2O + KCl$ section below.

XRD

Figure 5 shows XRD patterns acquired in dry $O_2 + KCl$. It may be noted that KCl was only detected after one and three hours, indicating that, with time, KCl is completely consumed by reaction and/or vaporization. K_2CrO_4 was detected after

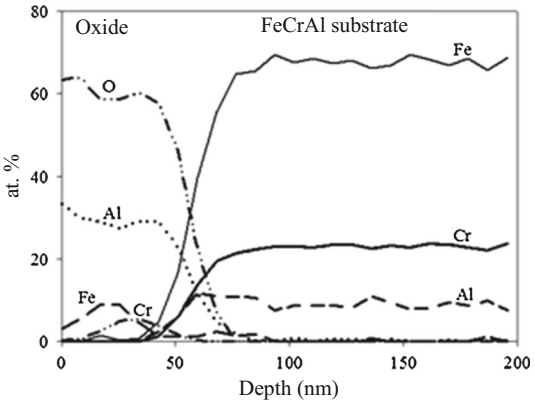

Fig. 2 AES depth profile of Kanthal® AF exposed to $O_2 + H_2O$ at 600 °C for 168 h

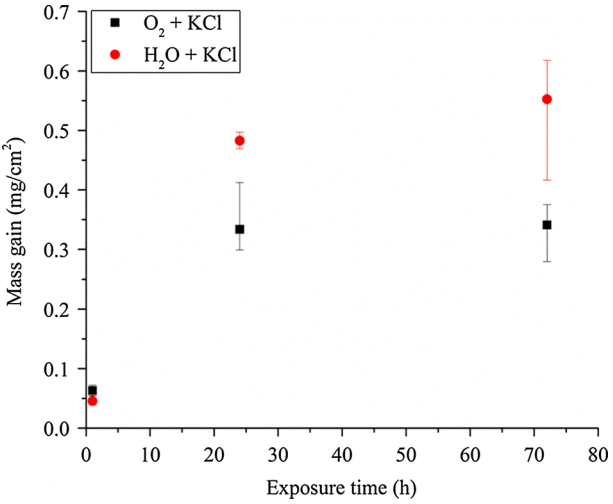

Fig. 3 Mass gain versus exposure time for Kanthal® AF exposed in a horizontal tube furnace at 600 °C in O_2 and $O_2 + H_2O$ in the presence of KCl

1, 3 and 72 h. Initially, the chromium-rich corundum-type oxide $(FeCr)_2O_3$ formed on the surface. With exposure time, the corresponding peak positions shifted slightly toward the lower diffraction angle, indicating an increase in cell volume, which is attributed to the increase in the Fe content. After 72 h the positions of the main peaks corresponded to hematite (α-Fe_2O_3), representing the iron-rich end point of the solid solution $(FeCr)_2O_3$. However, after 72 h there was still some diffraction from chromium-rich $(FeCr)_2O_3$. After 3 and 24 h of exposure, a few additional weak diffraction peaks appeared that could not be attributed to specific compounds.

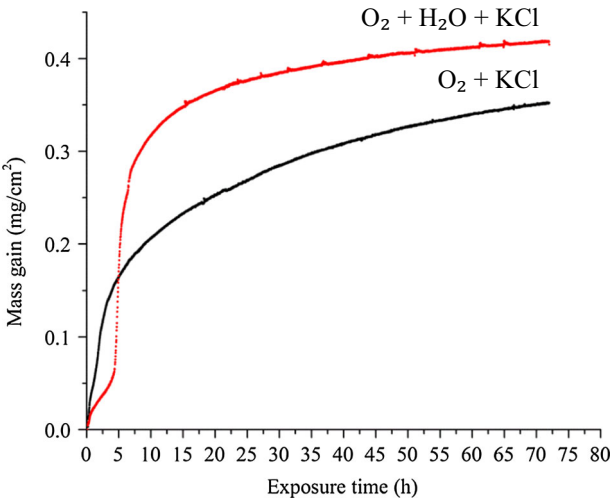

Fig. 4 In-situ TGA (mass gain vs. exposure time) for Kanthal® AF at 600 °C in O_2 and $O_2 + H_2O$ in the presence of KCl

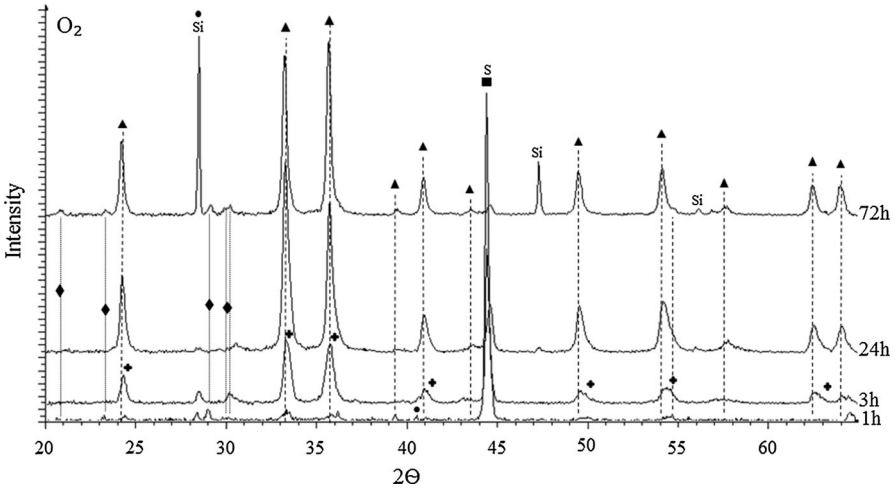

Fig. 5 XRD diffractograms for Kanthal® AF after 1, 3, 24 and 72 h at 600 °C in O_2 + KCl (Si was used as standard). The symbols indicate: K_2CrO_4 (*filled diamond*), (Fe_2O_3 (*filled triangle*), Cr_2O_3 (+), KCl (*filled circle*) and substrate (*filled square*)

IC

The IC results in Fig. 6 show that the amount of chloride on the samples decreases with exposure time in dry O_2. The chloride detected corresponds to 70, 54, and 20 % of the added amount after 1, 24 and 168 h, respectively. Figure 6 also shows the formation of chromate (VI) on the samples. The maximum amount

of CrO_4^{2-} that can form on the surface (considering that all KCl added before exposure is converted to potassium chromate, see Reaction (1)) is 0.33 μmol/cm^2. The amount of chromate detected on the surface was 33 % of the theoretical yield after 1 h and 52 % after 24 h. The amount of chromate decreased after longer exposure times.

SEM/EDX

SEM/EDX analysis after 1 h of exposure to O_2 + KCl (Fig. 7) showed a thin oxide that covered most of the surface. Much of the thin oxide features 1–10 μm irregularly shaped corrosion product particles on top of the surface. EDX showed chlorine but no potassium in these particles, suggesting that they consist of chlorides formed by the alloying elements (Fe, Cr, Al). Corrosion product agglomerates with 10–100 μm diameters are assumed to have replaced the KCl crystals present before exposure because they showed the same distribution and size and similar shape. They were dominated by iron oxide with some Cr and Al. The shell-like structures that mimic the shape of the original salt crystals are assumed to correspond to partly reacted KCl crystallites (the latter type is shown in the BSE image in Fig. 7). In addition there were rounded corrosion product agglomerations with a diameter of 5–20 μm. The EDX analyses showed that they were dominated by O, Fe, Cr and K and contained very little Cl.

After 3 h in O_2, most of the thin oxide had been replaced by a rough base oxide that was dominated by iron and also contained considerable amounts of Cr and some Al (Fig. 8). Notably, the Cl-containing corrosion product particles that were so conspicuous after 1 h are rarely seen at this stage. However the corrosion product agglomerates and shell-like structures seen after 1 h remained on the surface after 3 h of exposure. EDX analyses showed that these features have a composition similar to that of the rough base oxide. In the middle of Fig. 8 there are a small number of unreacted KCl crystals. Spherical 5–20 μm diameter corrosion product agglomerations were also present at this stage. They are similar to the corresponding features seen after 1 h but poorer in potassium. In addition, there was a small amount of particles in the size range of 1–3 μm on the scale surface (not shown). EDX point analyses showed that they mainly contained K, Cr and O, which lead to the inference that they consisted of K_2CrO_4, which was supported by XRD (see Fig. 5). The presence of chromate was also verified by the IC analysis (Fig. 6).

Figure 9 shows EDX maps of the corroded surface after 24 h in dry O_2. The oxide morphology is similar to the one described after 3 h. The main difference is that patches of iron-rich oxide have formed around the former KCl crystals (not shown). In some cases several of these patches have merged, forming larger areas. Al and Cl can be seen in the areas with a thinner oxide scale in Fig. 9, while iron is the dominant cation in the areas covered by a thick scale. The EDX maps also show a few small particles mainly containing K, Cr and O, which have been concluded to be K_2CrO_4. The corrosion product agglomerates contain O, Cr, Fe and Al (about 4 at.% Al, 16 at.% Cr and 22 at.% Fe). The Cl detected by EDX is not correlated to

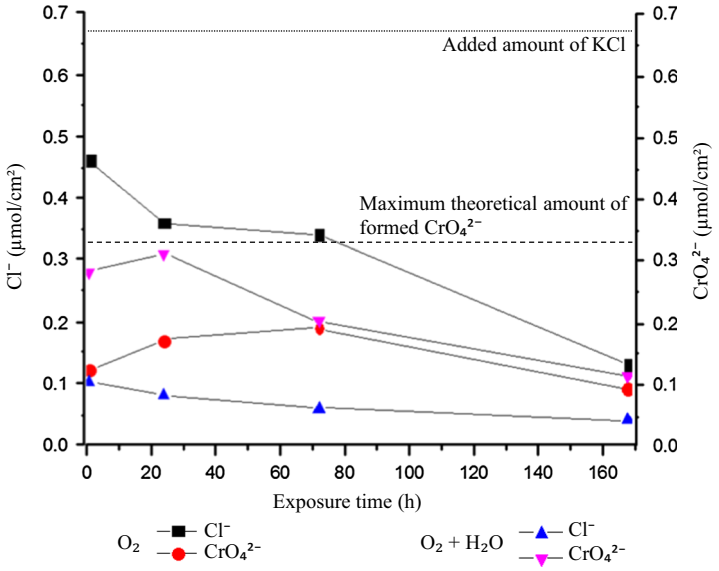

Fig. 6 Amount of water soluble ionic substances on the sample surface versus exposure time for Kanthal® AF exposed at 600 °C in O_2 and in $O_2 + H_2O$ in the presence of KCl

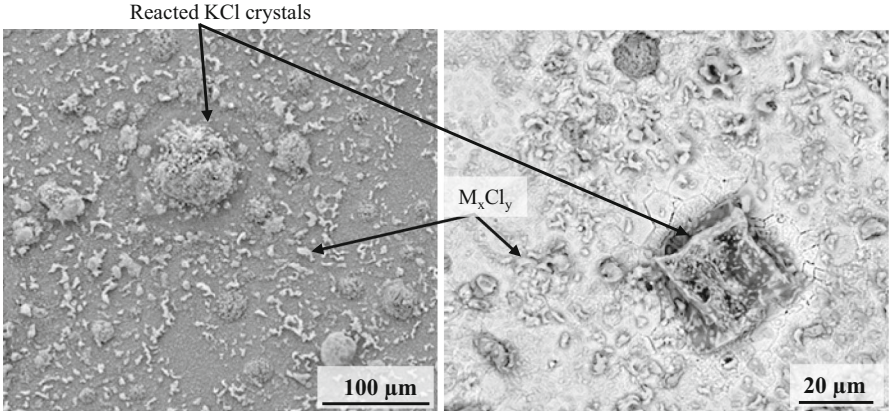

Fig. 7 SEM images (SE *left* and BSE *right*) of Kanthal® AF exposed at 600 °C for 1 h in O_2 with KCl

K, which shows that it does not correspond to KCl. Figure 10 is a high-magnification image of the boxed area in Fig. 9 which contains chlorine according to EDX analysis. The Cl-enriched areas appear smooth and bright in the BSE and SE images in Fig. 10 and are also rich in Cr. Since potassium is absent it has been concluded that the Cl is present in the form of chlorides of the alloying elements. The bright angular particles in Fig. 10 consist of iron chromium oxide.

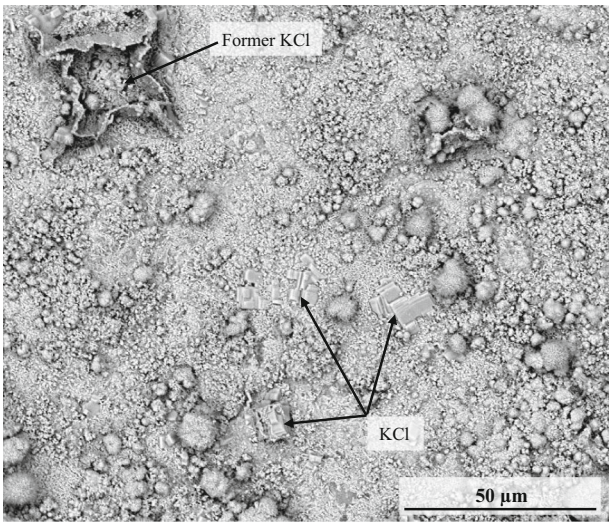

Fig. 8 SEM-BSE image of Kanthal® AF exposed at 600 °C for 3 h in O_2 with KCl

Figure 11 shows a cross section of scale and substrate after 24 h of exposure in dry O_2. The scale is porous and multi-layered and there is an oxidation-affected zone in the alloy substrate. The EDX analysis in Fig. 12 (showing a limited area of Fig. 11) reveals a succession of four sub-scales on top of each other. Each sub-scale features a more or less continuous thin layer made up of oxides of Al, Fe and Cr. It is proposed that each of these thin layers corresponds to an external scale that was once protective. According to EDX spot analysis the outermost thin layer has higher aluminium content than the thin layers closer to the substrate. The innermost thin layer is dominated by Cr and Fe. Obviously, only the innermost layer is still protective at this stage. In addition to the thin layers, there are large oxide agglomerations, especially in the outermost sub-scale, which correspond to the spherical oxide agglomerations seen in the top-view image in Fig. 9. They are dominated by relatively pure iron oxide but also feature smaller Cr-rich areas at the centre. Areas in the outer subscales exhibiting potassium but no chlorine are tentatively attributed to K_2CrO_4 (compare Fig. 9).

The Al and N EDX elemental maps overlap in the oxidation-affected zone immediately below the scale, indicating that aluminium nitrides have formed (see Fig. 12). Cl-enriched areas are found beneath the oxide subscale, which is still in contact with the substrate. Because of the absence of potassium, it has been deduced that these areas consist of chlorides of the alloying elements (Fe, Cr and Al). However, the data (including EDX point analyses) do not allow identification of specific compounds. It may be noted that the chlorides were formed close to the alloy grain boundaries. The same characteristic oxide morphologies (top view) were present after 72 h of exposure (not shown). As noted above, spallation occurred after 168 h.

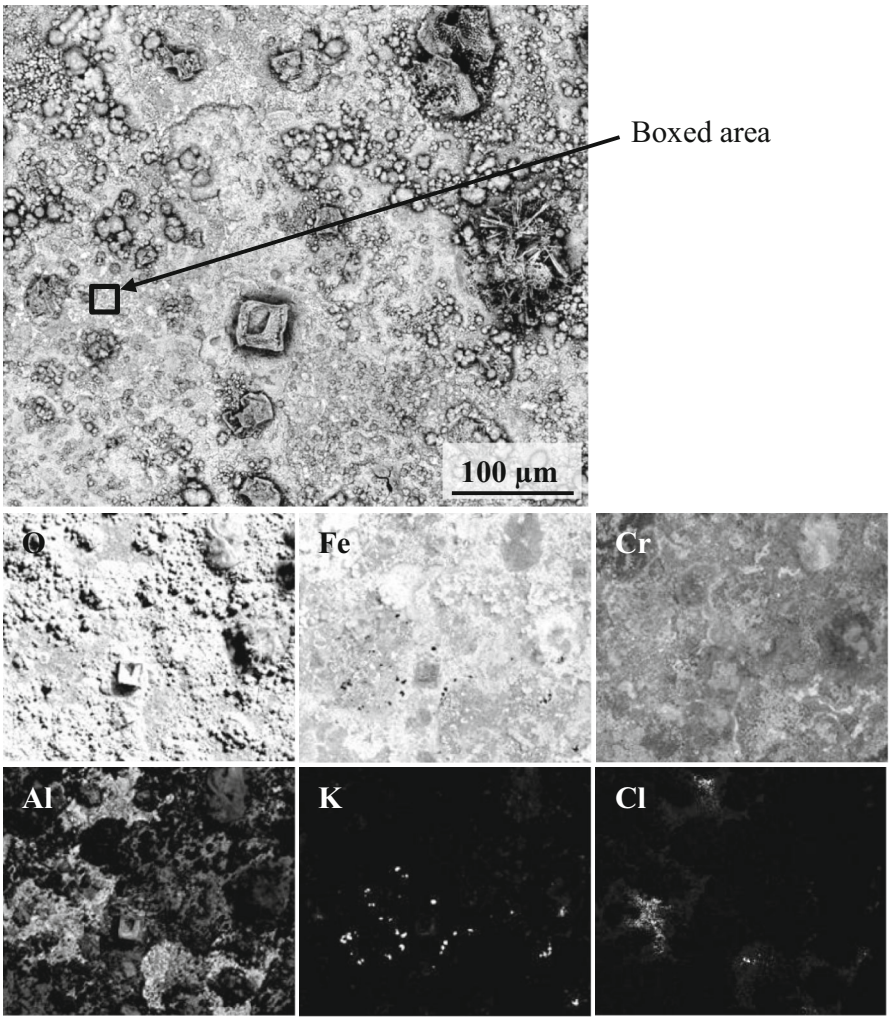

Fig. 9 SEM-BSE image and EDX elemental maps of Kanthal® AF exposed at 600° C for 24 h in O_2 with KCl

Oxidation in $O_2 + H_2O$ in the Presence of KCl

Gravimetry

According to Fig. 3 the mass gains in the ex situ $O_2 + H_2O + KCl$ and the $O_2 + KCl$ runs are similar. However, the in situ TG measurements in Fig. 4 reveal that the corrosion kinetics are rather different in the two environments. Thus, in $O_2 + H_2O + KCl$, the TG curve is linear between approximately 1 and 4 h. Subsequently, mass gain accelerated rapidly. After >10 h, the TG curve becomes rather flat. In dry O_2 there is no linear part of the TG curve.

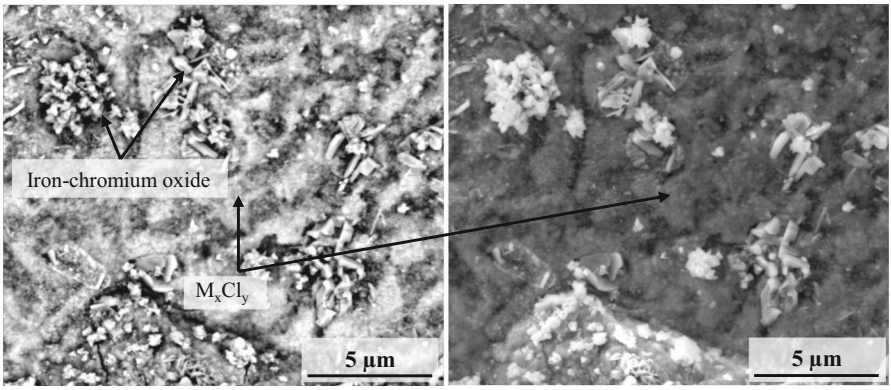

Fig. 10 SEM images (BSE *left* and SE *right*) of Kanthal® AF exposed at 600 °C for 24 h in O_2 with KCl

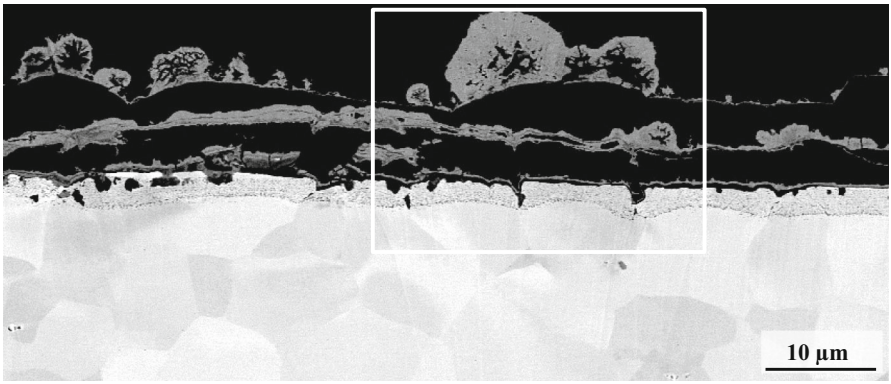

Fig. 11 SEM-BSE image of a BIB cross section of Kanthal® AF exposed at 600 °C for 24 h in O_2 with KCl

XRD

The same crystalline corrosion products were identified as in the corresponding dry exposure (compare Figs. 5, 13). K_2CrO_4 was detected after all exposure times except at 168 h (not shown). The K_2CrO_4 peak intensities were higher here than in the dry exposures. Similar to the corresponding dry runs, the $(FeCr)_2O_3$ solid solution became more iron-rich with time and hematite (α-Fe_2O_3) and Cr rich $(FeCr)_2O_3$ solid solution appeared after 72 h. In contrast to the dry exposures, there were no unidentified peaks in the diffractograms.

IC

The IC analyses showed that the chloride added before exposure was lost more rapidly than the corresponding dry O_2 runs, see Fig. 6. The formation of chromate

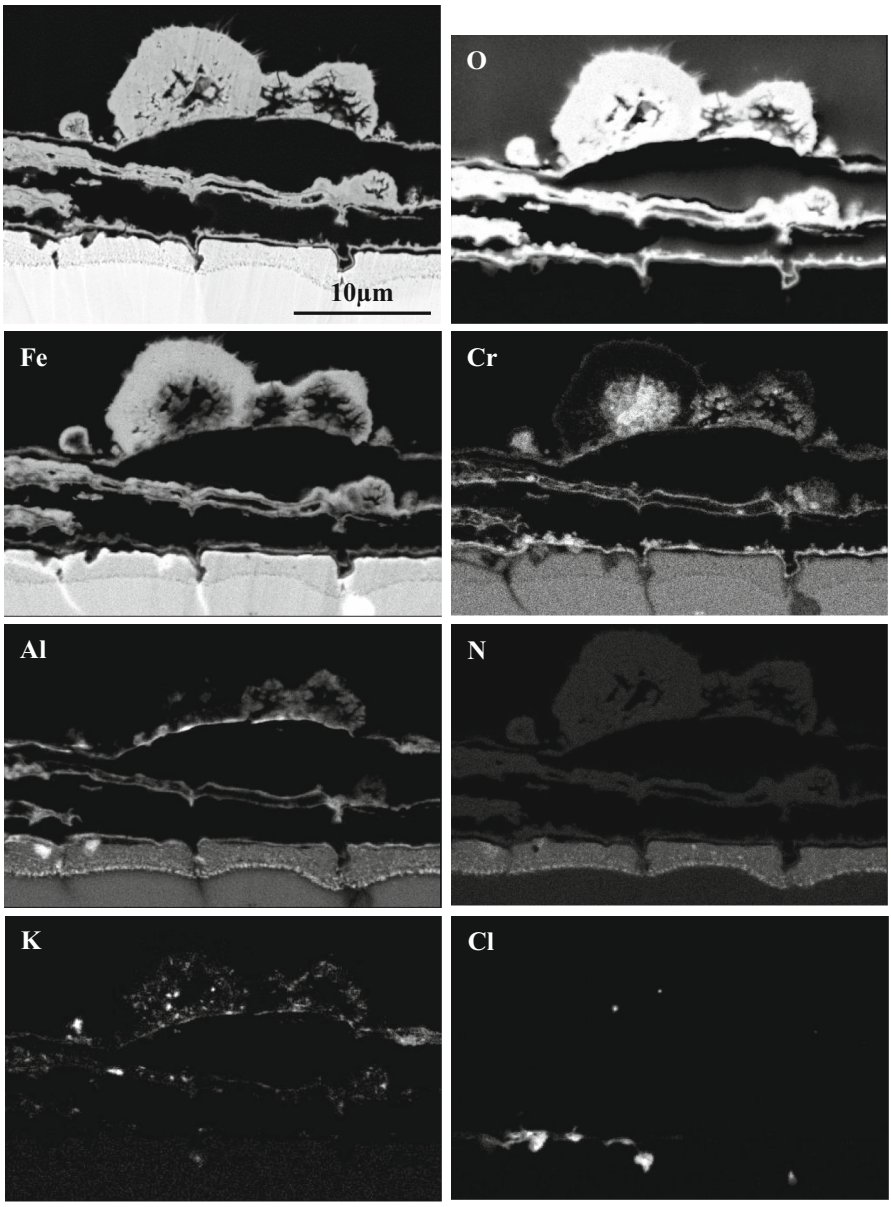

Fig. 12 SEM-BSE image and EDX elemental maps of a BIB cross section of Kanthal® AF exposed at 600° C for 24 h in O_2 with KCl

(VI) on the surface was also much faster than in dry O_2 (see Fig. 6). Already after 1 h, 0.28 µmol of chromate was formed, corresponding to 85 % of the available potassium on the surface. After 24 h the amount of chromate formed reached 94 % of the theoretical yield. As in the dry O_2 experiment, the amount of chromate

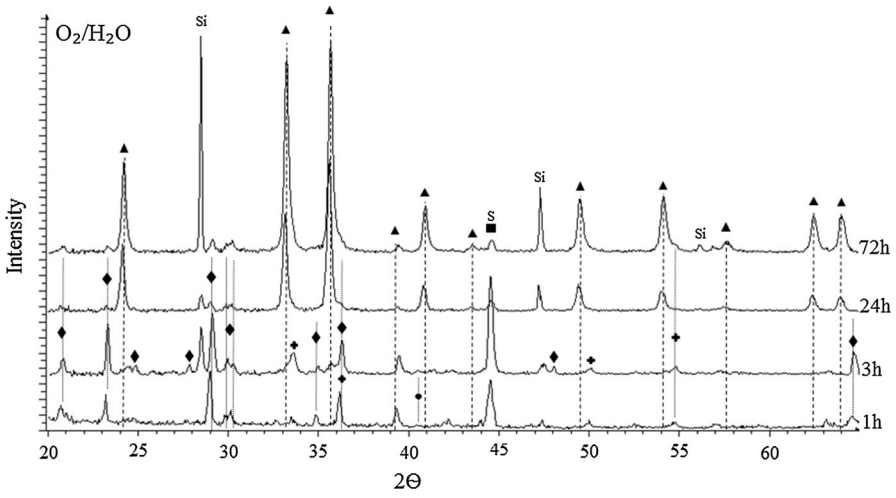

Fig. 13 XRD diffractograms for Kanthal® AF after 1, 3, 24 and 72 h at 600 °C in $O_2 + H_2O + KCl$ (Si is used as standard). The symbols indicate: K_2CrO_4 (*filled diamond*), (Fe_2O_3 (*filled triangle*), Cr_2O_3 (+), KCl (*filled circle*) and substrate (*filled square*)

decreased >24 h. The IC analysis (see Fig. 6, Table 2) showed that the formation of CrO_4^{2-} and the consumption of chloride on the metal surface were, in most cases, in accordance with the stoichiometry of the reaction:

$$2KCl(s) + 1/2Cr_2O_3(s) + H_2O(g) + 3/4O_2(g) \rightarrow K_2CrO_4(s) + 2HCl(g) \qquad (1)$$

The stoichiometric relationships in Table 2 show that other mechanisms for chloride loss from the surface, such as KCl volatilization, are comparatively slow. It can be concluded that the Cl that remained on the surface (15 % after 1 h and 6 % after 168 h) was present either as unreacted KCl or as chlorides of Al, Fe or Cr. When spallation occured (168 h) most of the chloride was already lost from the samples, and therefore spallation hardly affected the chlorine balance. Table 2 shows large deviations from the stoichiometry of Reaction (1) after long exposure times, suggesting that K_2CrO_4 decomposes with time.

SEM/EDX

After 1 and 3 h much of the surface was still covered with a thin and smooth oxide scale, the alloy grain boundaries were still visible, (Figs. 14, 15). While the thin oxide is similar to the one formed under dry conditions after 1 h (see Fig. 7), its surface has been covered with potassium chromate particles, and there is little evidence for the chloride-containing corrosion product particles formed in dry conditions. It may be noted that while the thin oxide was replaced by a thick iron-rich oxide after 3 h in dry conditions, it remained intact in the wet environment at that stage (Fig. 15). The K_2CrO_4 particles were much more numerous and no unreacted KCl crystals were observed on the surface. This is in accordance with the

Table 2 Water-soluble anions after exposure in O_2 and $O_2 + H_2O$ (μmol/cm^2) and stoichiometry of Reaction (1)

Exposure environment	Time (h)	Cl^-	CrO_4^{2-}	$\frac{(n_{Cl^-} + 2n_{CrO_4^{2-}})}{n_{applied\ K}}$
O_2	1	0.46	0.12	1.04
O_2	24	0.36	0.17	1.04
O_2	72	0.34	0.19	1.07
O_2	168	0.13	0.09	0.46
$O_2 + H_2O$	1	0.10	0.28	0.99
$O_2 + H_2O$	24	0.08	0.31	1.04
$O_2 + H_2O$	72	0.06	0.20	0.69
$O_2 + H_2O$	168	0.04	0.11	0.39
Amount of KCl added before exposure:				0.67 μmol/cm^2
Theoretical yield of CrO_4^{2-}				0.33 μmol/cm^2
$n_{applied\ K}$				0.67 μmol/cm^2

IC analysis (see above), which shows that the formation of CrO_4^{2-} is faster in $O_2 + H_2O$ environment. The distribution of the K_2CrO_4 crystallites is clearly seen in the EDX maps of Fig. 15. Similar to the dry O_2 case, the original KCl crystals were replaced by corrosion product agglomerations and shell-like formations. In the wet environment, the latter type dominates and corrosion product agglomerates only formed in connection to the largest KCl crystals. Figure 15 also reveals that Cl is enriched at the alloy grain boundaries, indicating that part of the KCl added has formed chlorides with the alloying elements. It was not possible to identify the specific metal chlorides due to the large interaction volume of the EDX analysis.

After 24 h, the surface morphology was similar to that in the dry O_2 environment, i.e. most of the surface had been covered with a rough iron-rich base oxide containing corrosion product agglomerations formed at the former KCl crystals (compare Figs. 9, 16). Thus, there are almost no areas with the thin smooth base oxide as found after 3 h (compare Figs. 15, 16). Substantial amounts of K_2CrO_4 particles remain after 24 h (see Fig. 16). At this stage, no chlorine was detected using EDX, which implies that KCl is absent. However, the presence of small amounts of chlorides of Al, Cr and Fe below the oxide scale cannot be ruled out.

A cross-sectional image shows that the oxide scale formed in the $O_2 + H_2O$ environment is much more compact than that formed in the dry O_2 environment (Figs. 11, 17). Similar to the dry exposure, the oxide scale is layered. K_2CrO_4 particles are situated at the scale/gas interface, immersed in oxide. The EDX point analysis shows that the upper part of the scale mainly consists of iron oxide. It is suggested that this part corresponds to α-Fe_2O_3, which was identified using XRD (Fig. 13). In the middle of the outer (iron oxide) part of the scale there is a band enriched in aluminium and poor in chromium. This band is suggested to correspond to the initial thin and smooth base oxide observed in top-view after 3 h (Fig. 15). The lower part of the oxide scale is relatively rich in Cr and Al (roughly 18 at.% Fe,

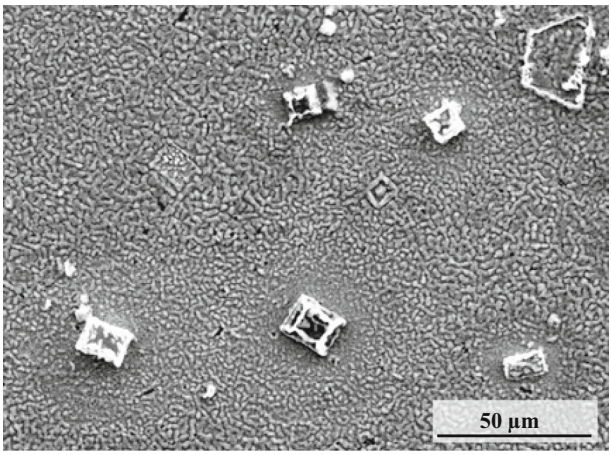

Fig. 14 SEM-SE image of Kanthal® AF exposed at 600 °C for 1 h in $O_2 + H_2O$ with KCl

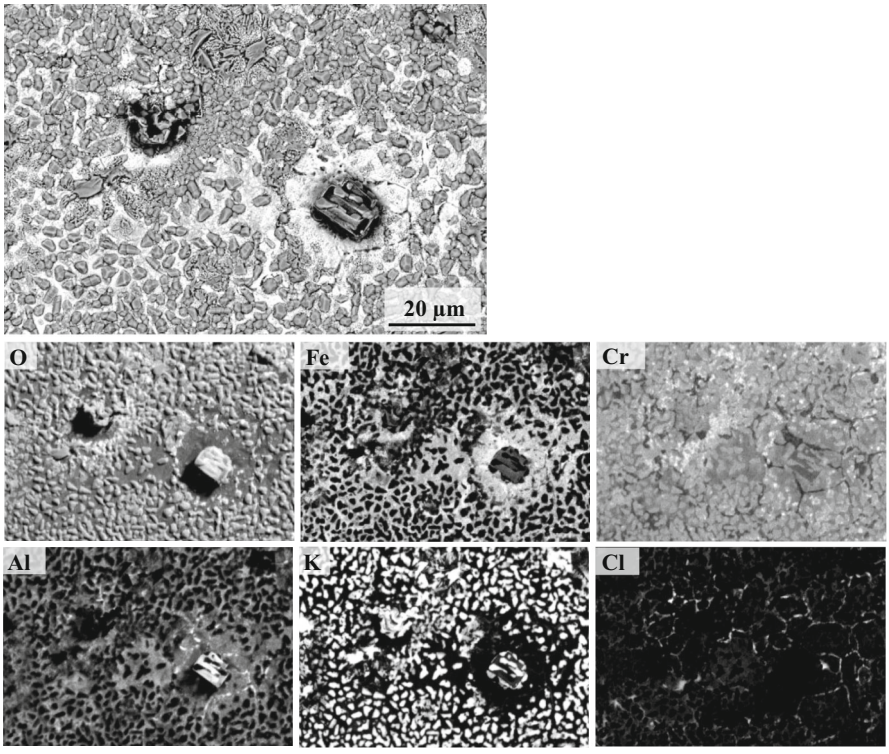

Fig. 15 SEM-BSE image and EDX elemental maps of Kanthal® AF exposed at 600° C for 3 h in $O_2 + H_2O$ with KCl

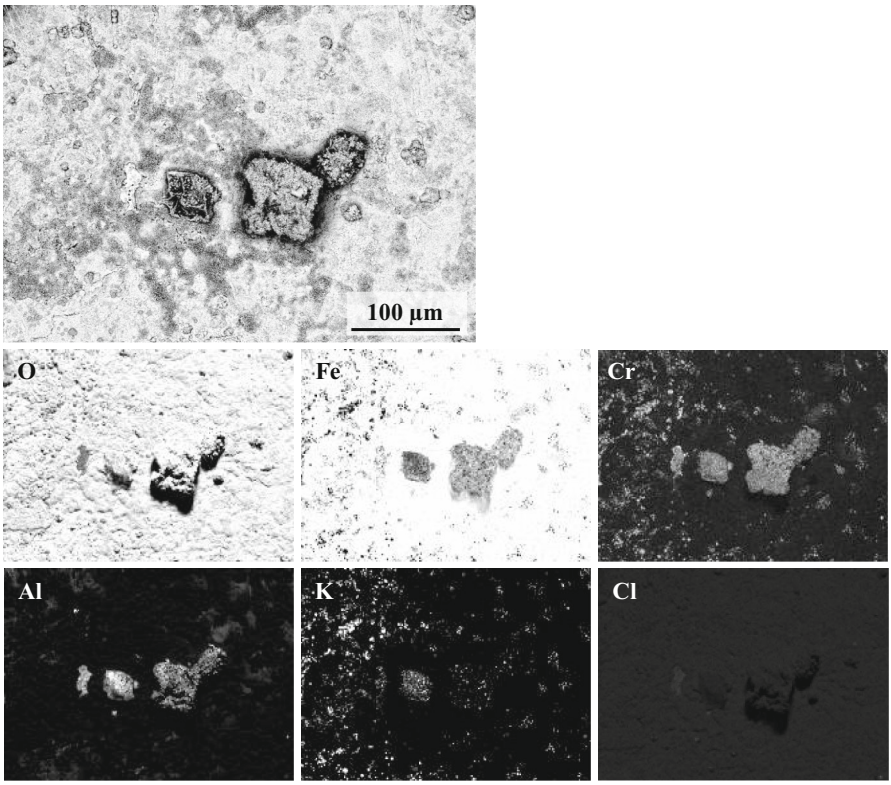

Fig. 16 SEM-BSE image and EDX elemental maps of Kanthal® AF exposed at 600° C for 24 h in $O_2 + H_2O$ with KCl

18 at.% Cr and 4 at.% Al). Similar to the dry O_2 exposure, the substrate below the scale has been enriched in nitrogen, indicating that alloy nitridation has occurred. In accordance with the plan view SEM/EDX, no chlorine was detected in the scale. This implies that the chlorides formed by the alloy constituents (see the 3 h results above) are no longer present.

The oxidation morphology after 72 h is similar to that seen after 24 h, except that the amount of K_2CrO_4 particles on the surface has decreased (see SE image Fig. 18). At this stage a small part of the surface is still covered by a relatively thin base oxide, see the SEM image in Fig. 18. An enlargement of the area marked by the small square (Fig. 18) reveals small patches with oxide whiskers. The distribution and shape of these patches are reminiscent of the K_2CrO_4 particles seen at an earlier stage. The EDX maps show that the patches are enriched in Cr and O. Small amounts (roughly 2 at.%) of K were also present which may correspond to unreacted K_2CrO_4.

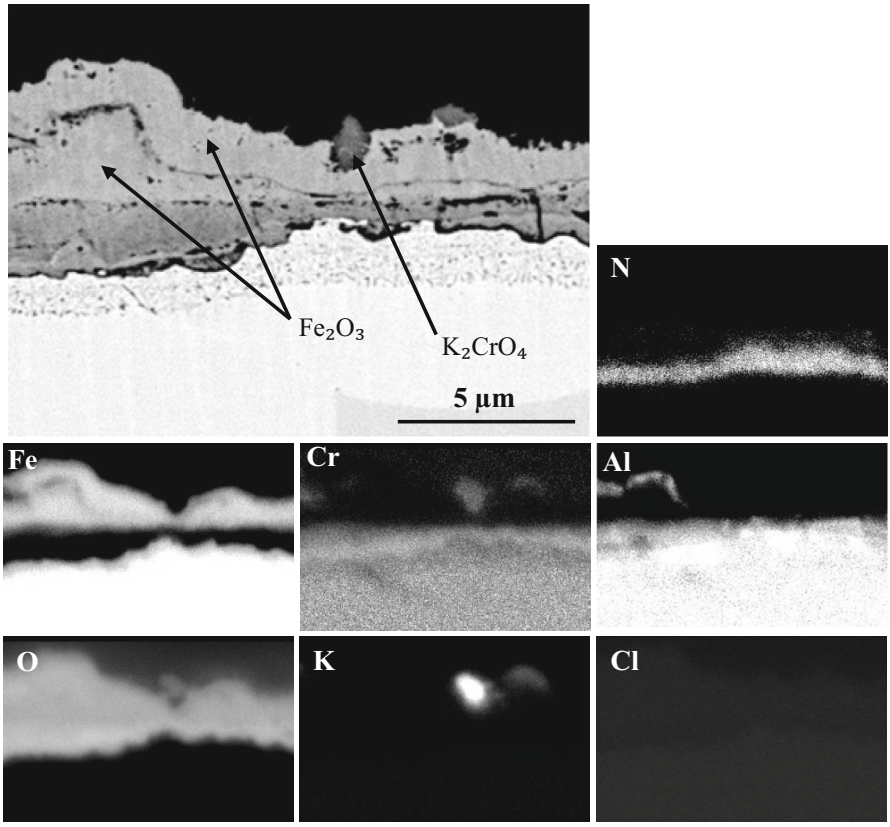

Fig. 17 SEM BSE image and EDX elemental maps of a BIB cross section of Kanthal® AF exposed at 600° C for 24 h in $O_2 + H_2O$ with KCl

Discussion

Oxidation in the absence of KCl resulted in an oxide film dominated by alumina, the aluminium content increasing with exposure time. There was a chromia band in the middle of the oxide film and iron was enriched in the top part (Fig. 2). The chromia band corresponds to Cr_2O_3 which was identified using XRD while the alumina in the film was apparently non-crystalline. This is in accordance with a recent study of Canovic et al. [20] who reports that the oxide film formed on Kanthal® AF in O_2 and $O_2 + H_2O$ at 600 °C consists of a top corundum-type layer and a bottom layer made up of non-crystalline alumina. A TEM investigation by Liu et al. [21] of the oxide film formed on Kanthal® AF after 1 h in dry O_2 at 900 °C showed that the oxide film (<100 nm) exhibited a central, chromium enriched band and an outer Fe enriched zone. In contrast to the present study, where the only crystalline compound identified was Cr_2O_3, γ- and α-alumina were identified by Liu et al. [21]. Similar to Liu et al. [21], it is suggested that Cr and Fe enter the oxide film during transient oxidation, i.e., during sample heat-up.

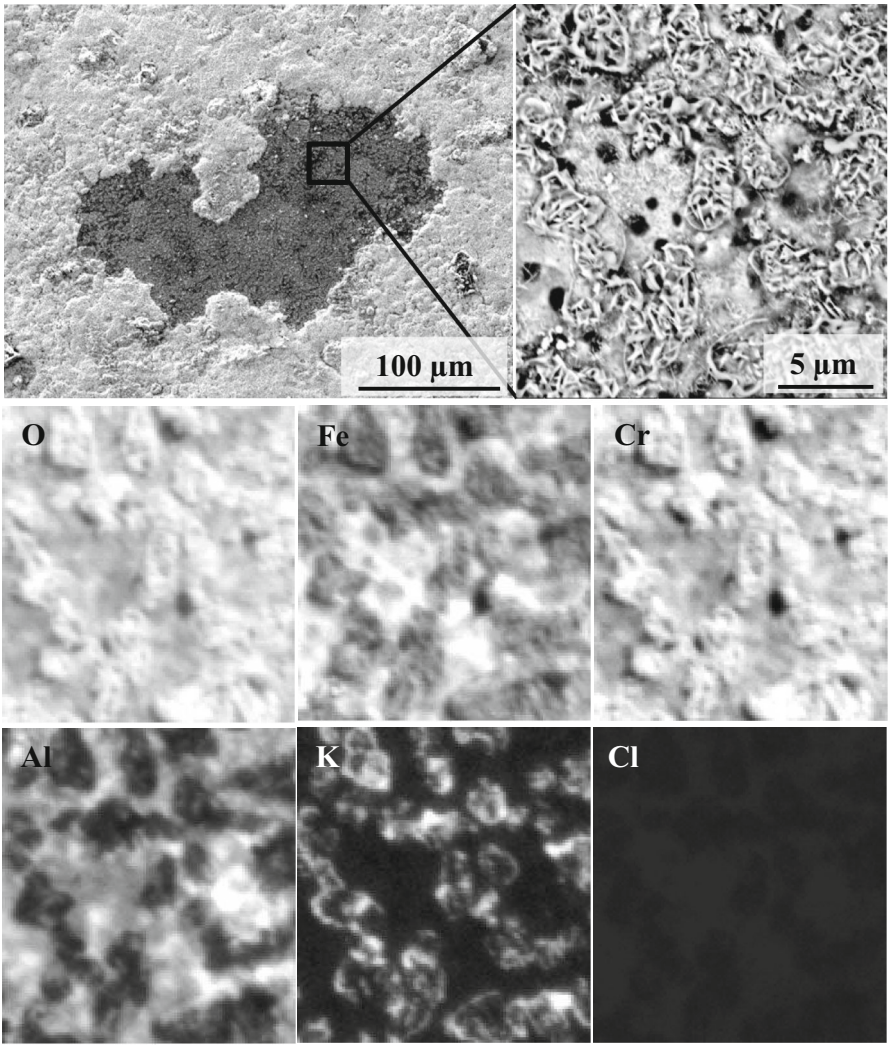

Fig. 18 SEM images (SE *left* and BSE *right*) and EDX elemental maps of Kanthal® AF exposed at 600° C for 72 h in $O_2 + H_2O$ with KCl

The evidence from SEM/EDX, XRD and IC clearly shows that KCl reacts to form K_2CrO_4 on the alloy surface. As noted in the introduction, FeCrNi and FeCrAl alloys have been reported to react with KCl and water vapour to form K_2CrO_4 [7, 8, 13, 14] according to Reaction (1). For standard state conditions it is found that $\Delta G^{\circ}_{873K} = 90.5$ kJmol^{-1}K [22] for Reaction (1). The corresponding equilibrium partial pressure of HCl (P_{eq}(HCl)) is 400×10^{-6} atm under the experimental conditions ($pO_2 = 0.05$ atm, $pH_2O = 0.40$ atm). The continuous flow of gas ensures that p(HCl) << P_{eq}(HCl) during the experiment. Hence, Reaction (1) is

expected to proceed from left to right. The formation of K_2CrO_4 in a dry O_2 environment is less favoured:

$$1/2Cr_2O_3(s) + 2KCl(s) + 5/4O_2(g) \rightarrow K_2CrO_4(s) + Cl_2(g) \quad (2)$$

for which $\Delta G^{\circ}_{873K} = 90.8$ kJmol^{-1}K [22], corresponding to $P_{eq}Cl_2 = 0.09 \times 10^{-6}$ atm (in 5 % O_2). It may be noted that the "dry" O_2 environment contained on the order of 10 ppm water vapour, corresponding to a P_{eq}(HCl) of 1.5×10^{-6} atm by Reaction (1). This implies that K_2CrO_4 formation is dominated by Reaction (1) even in the dry exposures and that Reaction (2) is of secondary importance.

When the material is exposed in the presence of KCl, the salt is initially separated from the alloy by an air-formed film, only a few nanometres thick, consisting of oxides and hydroxides. During heat-up, this film increases in thickness and the hydroxides form oxides. It has been reported by Pettersson et al. that the formation of K_2CrO_4 in Reaction (1) proceeds at a measurable rate from 400 °C [23]. Thus, chromate is expected to form as early as during sample heat-up. At this stage, the oxide is expected to be quite thin (between 3 and 30 nm), and relatively poor in Al. It is suggested that the protective properties of this film are compromised because of the consumption of chromia through Reaction (1) and that this leads to an increase in the oxidation rate of the alloy. The corrosion-accelerating effect of KCl is illustrated by the fact that the number of moles of CrO_4^{2-} detected after 1 h in $O_2 + H_2O$ was about 20 times greater than the number of moles of Cr present in the oxide film formed in the absence of KCl, after the same exposure time. Thus, chromium was oxidised more rapidly in the presence of KCl.

The observation that CrO_4^{2-} formation was much faster in $O_2 + H_2O$ compared to dry O_2 (see Fig. 6) is in accordance with the K_2CrO_4 formation being dominated by Reaction (1). According to the IC analysis (Table 2), the ratio between formation of chromate (VI) and the amount of chloride lost from the surface satisfies the stoichiometry of Reaction (1) in both dry and wet environments after short exposure times. Consequently, the formation of chromate was accompanied by the loss of chlorine in the form of HCl(g). In addition, it can be concluded that the loss of Cl from the surface by other mechanisms such as evaporation of KCl and transition metal chlorides (see below), is initially of secondary importance.

Under dry conditions, chlorides of the main alloy constituents were observed after 1, 3 and 24 h. In the presence of water vapour, metal chlorination was observed after 1 and 3 h, but not after 24 and 72 h. In other words, the amount of solid chlorides formed was much less than in the dry O_2 environment, e.g. the chloride-containing corrosion product formed on top of the thin oxide in dry O_2 was absent in the presence of $O_2 + H_2O$. Thus, metal chlorination is much more prominent in a dry environment than in a wet one. It is argued that this is mainly because of Reaction (1), which causes Cl to be lost from the surface in the form of HCl under humid conditions. As observed, chromate formation was slow in "dry" condition, allowing KCl longer time to interact with the alloy. This argument is fully supported by the IC analyses (see Table 2 and Fig. 6).

The TG curves in Fig. 4 further illustrate the different corrosion kinetics in dry and wet environments. It may be noted that the overall mass change is the result of

several processes, including oxide growth, the potassium chromate formation by Reaction (1), alloy chlorination, and volatilization of KCl and metal chlorides. The initially relatively slow mass gain in wet condition was attributed partly to the rapid loss of HCl(g) in Reaction (1), and partly by the slower corrosion attack. Considering the small amount of KCl added (corresponding to 24 μg/cm^2 of Cl^-) most of the difference should be due to the faster oxidation in dry condition (compare the situation after 3 h in Fig. 8 (dry) and Fig. 15 (wet)). In wet condition mass gain was relatively slow between approximately 1 and 4 h. At this stage chromate formation (Reaction (1)) occurred on the surface which was still protected by a Cr-rich scale. The accelerated mass gain that sets in after about 5 h and then lasts a few hours was attributed to the formation of a rapidly growing iron oxide scale, i.e. breakaway oxidation. The TG curve in dry condition provided little indication of protective behaviour.

The kinetics of the corrosion process can be further elucidated by displaying the mass gain data on a ln(m) versus ln(t) plot (Fig. 19). Assuming that mass gain is proportional to exposure time, the slope in such a plot will correspond to 1/α, where α is the exponent in the kinetic Eq. (3), a constant mass gain corresponding to $\alpha = 1$, and parabolic oxidation, giving $\alpha = 2$.

$$m^{\alpha} \propto t$$

$$\alpha \ln(m) \propto \ln(t)$$

$$\ln(m) \propto (1/\alpha) \ln(t) \tag{3}$$

The two ln(m) versus ln(t) plots in Fig. 19 display several similarities. The large scatter during the first few minutes after reaching the exposure temperature is attributed to the buoyancy effect. After this stage, there follows a short period during which α was 0.6 in dry and 1.0 in the wet environment, corresponding to accelerated and linear mass gain, respectively. Then comes a stage where α was about 2.0 corresponding to a period with relatively slow mass gain in the $O_2 + H_2O$ TG curve (Fig. 4). It may be noted that while Fig. 19 gives clear evidence of such a stage also in the dry O_2 environment, it was difficult to trace in the corresponding TG curve in Fig. 4. The subsequent breakaway behaviour in $O_2 + H_2O$ (Fig. 4) corresponds to a sudden decrease in the value of α to 0.1. Again, Fig. 19 reveals that there occurred a similar; although less marked transition in dry O_2. During the last stage of the exposure, the value of α was greater in $O_2 + H_2O$ than in dry condition, indicating that a more protective scale has evolved in the former case. This is supported by the cross-sectional micrographs, which showed a dense oxide scale in $O_2 + H_2O$ while a more porous layered scale formed in dry O_2 (see Figs. 11, 17).

The results suggest that we are dealing with two main corrosion modes, namely (I), breakaway oxidation triggered by chromate formation which is dominant in the $O_2 + H_2O$ environment and (II), chlorination of the alloy by KCl accompanied by rapid oxidation, which is predominant in dry O_2. In the $O_2 + H_2O$ environment, chromate formation in Reaction (1) depletes the protective scale in Cr, triggering the

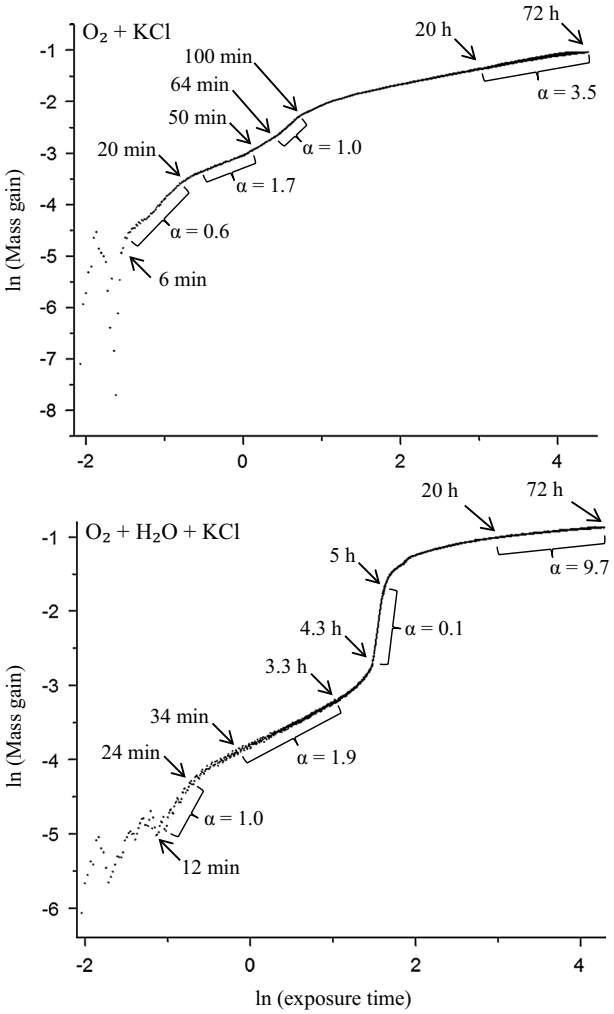

Fig. 19 ln(m) versus ln(t) of in situ TGA (mass gain vs. exposure time) for Kanthal® AF at 600 °C in O_2 and $O_2 + H_2O$ in the presence of KCl

formation of a fast-growing iron oxide scale. On the other hand, the concomitant loss of Cl from the surface in the form of HCl(g) decreases the tendency for chlorination of the substrate. In dry conditions, the KCl stays on the surface for a longer time, resulting in a higher degree of alloy chlorination. Thus, it is suggested that alloy chlorination results in the porous multi-layered oxide scales observed in dry O_2 (Fig. 11), while breakaway is caused by the formation of chromate (Reaction (1)) and results in a relatively dense scale, as observed in the presence of water vapour (Fig. 17).

The chlorination of high temperature steels by HCl, KCl and NaCl in the presence of O_2 at high temperatures has been investigated by several authors [5, 9,

13, 24]. Grabke et al. [9] proposed that alkali chlorides "catalyse" corrosion in the following way: First, the chlorine-containing species react to form Cl_2 at the scale/gas interface. Gaseous Cl_2 then penetrates the scale and reacts with the alloy substrate, forming chlorides. The (transition metal) chlorides are then transported (as gas molecules) to the scale surface via cracks and pores in the scale. At the scale surface they react with O_2 to form metal oxide and Cl_2. In this way, Cl_2 is regenerated, closing the so called "chlorine cycle".

The "chlorine cycle" scenario has some problems. First, the reactions proposed by Grabke et al. [9] and Li et al. [13] for generating Cl_2 at the scale surface appear unable to generate the necessary Cl_2. Thus, of the reactions proposed by Li et al. [13], the most favoured one is Reaction (2) (see above) which generates an equilibrium partial pressure of only 0.09×10^{-6} atm Cl_2 (at 5 % O_2). In the present case, where the alloy may form an alumina scale, we must examine whether or not the reaction of KCl, O_2 and Al_2O_3 can generate appreciable Cl_2 concentrations. The following reaction is considered:

$$2KCl(s) + Al_2O_3(s) + 1/2O_2(g) \rightarrow 2KAlO_2(s) + Cl_2(g) \quad (4)$$

$\Delta G^{\circ}_{873K} = 197.091$ kJmol^{-1}K [22], $P_{eq}\ Cl_2(g) = 3.6 \times 10^{-13}$ atm.

As the equilibrium concentrations of Cl_2 generated in (4) is quite low it is concluded that there is no viable route for generating Cl_2 for the chlorine cycle mechanism.

Another problem with the "chlorine cycle" is the inward transport of Cl_2 to the metal/scale interface where low oxygen activity is postulated to prevail. It is argued that the low oxygen activity at the metal/scale interface would be very difficult to maintain, considering that the cracks and pores open to Cl_2 diffusion must also be open to O_2 diffusion. Moreover, it is considered improbable that the highly reactive chlorine molecule would be able to reach the metal/scale interface without being reduced by the oxide en route (e.g. by Fe^{2+} ions in the scale). Further, because the chlorine cycle mechanism predicts that the metal chloride will form below the scale, it cannot account for the observation in the present paper that metal chlorides also form at the scale/gas interface. Similar observations have been made in the HCl-induced corrosion of FeCrNi steel at 500 °C in 5 % O_2 by Folkesson et al. [25].

It is argued that the problems inherent in the chlorine cycle mechanism can be resolved by applying an electrochemical mechanism for metal chlorination. Since Wagner [26, 27], the formation of external oxide scales on metals at high temperature is usually described in terms of an electrochemical mechanism where the oxidant (e.g. O_2) is reduced at the scale/gas interface while the metal is oxidized at the scale/metal interface, the two electrodes being connected by electronic and ionic currents:

$$1/2O_2 + 2e^- \rightarrow O^{2-} \quad (5)$$

$$Me \rightarrow Me^{2+} + 2e^-$$

.

In the case of the electrochemical chlorination of an alumina-forming alloy by KCl in the presence of O_2, the cathodic process on the scale surface should generate "free" chloride ions at the surface as well as incorporating potassium in a stable form. The analytical results show that as KCl is consumed, potassium becomes associated to Cr. The association of K and Cr is attributed to K_2CrO_4 which is mainly considered to be formed in Reaction (1). However, it is proposed that K_2CrO_4, also may form as part of the following electrochemical reaction:

Scale surface:

$$2KCl + 5/4O_2 + 1/2Cr_2O_3(s) + 2e^- \rightarrow K_2CrO_4(s) + 2Cl^-$$

Scale/alloy interface:

$$Fe(s) \rightarrow Fe^{2+}(oxide) + 2e^-$$

$$Cr(s) \rightarrow Cr^{2+}(oxide) + 2e^-$$

$$Al(s) \rightarrow Al^{3+}(oxide) + 3e^-$$

The sum reaction becomes (for the case of Fe oxidation):

$$2KCl(s) + 5/4O_2(g) + 1/2Cr_2O_3(s) + Fe(alloy) \rightarrow K_2CrO_4(s) + 2FeCl_2(s) \quad (6)$$

For Reaction (6), $\Delta G^{\circ}_{873K} = -141.458$ kJmol^{-1}K [22] which corresponds to a standard cell potential E^o of +0.73 V, thus showing that the reaction is strongly favoured by thermodynamics. The corresponding anodic reactions with Cr and Al provide even higher thermodynamic driving forces.

The electrochemical mechanism for metal chlorination by alkali chloride requires that the scale can conduct both ions and electrons. Cationic conduction through the scale is known to be dominated by the grain boundary transport at the experimental temperature [28]. Chloride ions do not dissolve in the bulk oxides of interest here. However, similar to hydroxide ions, chloride ions can exist in the adsorbed form, both on the scale surface and in the oxide grain boundaries. Thus, the ionic transport in the electrochemical cell is suggested to occur in the grain boundaries. In this scenario, the relative transport rates of chloride ions and metal ions would determine whether the solid chloride forms on top of the scale or at the scale/alloy interface.

The presence of metal chloride on the metal surface (see Figs. 7, 10) implies that non-equilibrium conditions prevail. This is not unexpected, considering the rapid corrosion process. Because of the high equilibrium vapour pressures at 600 °C (P_{eq} $FeCl_2(g) = 1 \times 10^{-3}$ atm, P_{eq} $CrCl_2(g) = 0.5 \times 10^{-6}$ atm) these compounds are expected to vaporize [22]. Accordingly, the transition metal chlorides on the surface are only seen after short exposure times. The observed metal chlorides on the surface (e.g. Figure 10) after 24 h might have a thin oxide layer closest to the

oxidising atmosphere. This has been observed by Jonsson et al. at 500 °C on a FeCrNi steel in the presence of HCl(g) [29].

The scale morphology after breakaway in the $O_2 + H_2O + KCl$ environment (see Fig. 17) is similar to the one observed on chromia-forming stainless steels exposed to KCl in the presence of water vapour [14]. Jonsson et al. [14] showed that the scale consisted of an outward growing hematite and an inward growing FeCr spinel oxide. However, further investigation is needed to determine the structure and composition of the oxide scale formed on Kanthal® AF. Breakaway oxidation triggered by alkali chromate formation has been described for chromia-forming steels [7, 8, 14]. It was concluded that K_2CrO_4 acts as a sink for chromia in the oxide, thereby transforming the protective Cr-rich oxide to rapidly growing iron oxide. The present work indicates that KCl has a similar, corrosion accelerating effect on FeCrAl alloys at 600 °C. The sub-scale formation of aluminium nitrides also shows that the scale formed after breakaway is permeable to N_2. The formation of AlN may obstruct the ability of the alloy to form a protective alumina scale since the reservoir of aluminium close to the metal/scale interface decreases. Aluminum nitride precipitates have been reported to form in FeCrAl alloys at 1,100–1,200 °C when the alumina scale failed during oxidising conditions [30].

Table 2 shows that the amount of chromate on the surface decreases >24 h and that the stoichiometry of Reaction (1) is only satisfied up to 24 h. As spallation is not an issue, this must be due to the decomposition of K_2CrO_4. The thermal decomposition of K_2CrO_4 according to:

$$K_2CrO_4(s) + H_2O(g) \rightarrow 1/2Cr_2O_3(s) + 2KOH(g) + 3/4O_2(g) \quad (7)$$

is considered insignificant at the relevant temperature ($\Delta G^{\circ}_{873K} = 357.7$ kJmol^{-1}K [22], corresponding to P_{eq} KOH $= 1.5 \times 10^{-21}$ atm (5 % O_2, 40 % H_2O)). In addition, no decomposition was observed when a small amount of K_2CrO_4 was placed on gold foil and exposed for 168 h under the experimental conditions. Instead it is proposed that K_2CrO_4 is cathodically reduced on the scale surface, the electrons being supplied by alloy oxidation:

$$K_2CrO_4(s) + H_2O(g) + 3e^- \rightarrow 1/2Cr_2O_3(s) + 2KOH(l) + 3/2O^{2-}$$

$$Cr(alloy) \rightarrow Cr^{3+} + 3e^-$$

$$\sum: \; K_2CrO_4(s) + H_2O(g) + Cr(alloy) \rightarrow Cr_2O_3(s) + 2KOH(l) \quad (8)$$

$\Delta G^{\circ}_{873K} = -231.4$ kJmol^{-1}K [22], corresponding to a standard cell potential E^o of +0.80 V. Here, the reduction of K_2CrO_4 on the scale surface is coupled to the oxidation of metallic chromium. The latter reaction can of course be replaced by the oxidation of iron or aluminium. Because O_2 is a stronger oxidant than K_2CrO_4 (thermodynamically speaking), chromate reduction on the scale surface through Reaction (8) is only possible if the oxygen electrode (5) is far from equilibrium.

It may be noted that the reduction of K_2CrO_4 at cathodically active sites at the surface causes alkaline conditions that allow chromate formation to occur through chemical oxidation (9) elsewhere in the scale. In this way, K_2CrO_4 catalyses alloy oxidation.

$$2KOH(l) + 3/4O_2(g) + 1/2Cr_2O_3(s) \rightarrow K_2CrO_4(s) + H_2O(g) \quad (9)$$

$\Delta G^{\circ}_{873K} = -217.9$ kJmol^{-1}K [22].

Conclusions

- KCl strongly accelerated the corrosion of Kanthal® AF in O_2 and $O_2 + H_2O$ environments at 600 °C. The protective alumina-rich oxide formed in the absence of KCl was replaced with a rapidly growing oxide scale dominated by iron and chromium when KCl was present.
- In an $O_2 + H_2O$ environment, chromia in the scale rapidly reacted with KCl, oxygen and H_2O forming K_2CrO_4 and gaseous HCl. Chromate formation depleted the protective scale in Cr, triggering the formation of a fast-growing iron-rich scale.
- Chromate formation also occurred in a dry O_2 environment but was slower.
- Parallel to chromate formation, the main alloying elements formed chlorides, both on top of and below the oxide scale.
- Alloy chlorination was more pronounced in a dry O_2 than in an $O_2 + H_2O$ environment. This is because chromate formation rapidly converts KCl to HCl(g) in the latter environment. Thus, KCl stays on the surface for a longer time in a dry O_2 environment, resulting in a higher degree of alloy chlorination.
- It is proposed that the chlorination reaction is electrochemical, involving the migration of chloride ions in the grain boundaries of the scale.
- KCl-induced corrosion in a dry O_2 environment resulted in the formation of a porous multi layered oxide scale. In contrast, KCl-induced corrosion in an $O_2 + H_2O$ environment resulted in a relatively dense oxide scale. The difference in behaviour was attributed to metal chlorination being more prominent under dry conditions.
- KCl-induced corrosion was accompanied by the formation of aluminium nitride precipitates in the alloy substrate.

Acknowledgments The work was performed within the Swedish High Temperature Corrosion Centre (HTC). The authors wish to acknowledge Helena Götlind and the support from Sandvik Heating Technology.

References

1. H. Asteman, J. E. Svensson and L. G. Johansson, *Oxidation of Metals* **57**, 193 (2002).
2. I. Panas, J.-E. Svensson, H. Asteman, T. J. R. Johnson and L.-G. Johansson, *Chemical Physics Letters* **383**, 549 (2004).
3. Y. Shu, F. Wang and W. Wu, *Oxidation of Metals* **51**, 97 (1999).
4. H. P. Michelsen, F. Frandsen, K. Dam-Johansen and O. H. Larsen, *Fuel Processing Technology* **54**, 95 (1998).
5. M. J. McNallan, W. W. Liang, S. H. Kim and C. T. Kang, International Corrosion Conference Series **NACE-6**, 316 (1983).
6. J. Pettersson, C. Petersson, H. Asteman, J. E. Svensson and L. G. Johansson, *Materials Science Forum* **461–464**, 965 (2004).
7. C. Pettersson, J. Pettersson, H. Asteman, J.-E. Svensson and L.-G. Johansson, *Corrosion Science* **48**, 1368 (2006).
8. C. Pettersson, J. Pettersson, H. Asteman, J. E. Svensson and L. G. Johansson, *Oxidation of Metals* **64**, 23 (2006).
9. H. J. Grabke, E. Reese and M. Spiegel, *Corrosion Science* **37**, 1023 (1995).
10. M. Montgomery and A. Karlsson, *Materials and Corrosion* **50**, 579 (1999).
11. H. P. Nielsen, F. J. Frandsen and K. Dam-Johansen, *Energy & Fuels* **13**, 1114 (1999).
12. Y. Shinata, *Oxidation of Metals* **27**, 315 (1987).
13. Y. S. Li, Y. Niu and M. Spiegel, *Corrosion Science* **49**, 1799 (2007).
14. T. Jonsson, J. Froitzheim, J. Pettersson, J.-E. Svensson, L.-G. Johansson and M. Halvarsson, *Oxidation of Metals* **72**, 213 (2009).
15. C. Pettersson, L.-G. Johansson and J.-E. Svensson, *Oxidation of Metals* **70**, 241 (2008).
16. H. Asteman and M. Spiegel, *Corrosion Science* **50**, 1734 (2008).
17. H. Josefsson, F. Liu, J.-E. Svensson, M. Halvarsson and L.-G. Johansson, *Materials and Corrosion* **56**, 801 (2005).
18. F. Liu, H. Gotlind, J. E. Svensson, L. G. Johansson and M. Halvarsson, *Oxidation of Metals* **74**, 11 (2010).
19. H. Asteman, R. Norling, J. E. Svensson, A. Nylund and L. Nyborg, *Surface and Interface Analysis* **34**, 234 (2002).
20. S. Canovic, J. Engkvist, F. Liu, H. Lai, H. Götlind, K. Hellström, J.-E. Svensson, L.-G. Johansso, M. Olsson and H. Halvarsson, *Journal of the Electrochemical Society* **157**, C223 (2010).
21. F. Liu, H. Götlind, J.-E. Svensson, L.-G. Johansson and M. Halvarsson, *Corrosion Science* **50**, 2272 (2008).
22. FactSage 6.2 (Databases: Fact53, ELEM, BINS).
23. J. Pettersson, J. E. Svensson and L. G. Johansson, *Oxidation of Metals* **72**, 159 (2009).
24. N. Folkeson, T. Jonsson, M. Halvarsson, L. G. Johansson and J. E. Svensson, *Materials and Corrosion* **62**, 606 (2011).
25. N. Folkeson, L.-G. Johansson and J.-E. Svensson, *Journal of the Electrochemical Society* **154**, C515 (2007).
26. C. Wagner, *Zeitschrift für Physikalische Chemie* **B21**, 25 (1933).
27. P. Kofstad, *High Temperature Corrosion*, (Elsevier Applied Science Publishers Ltd, London, 1988).
28. D. J. Young, *High Temperature Oxidation and Corrosion of Metals*, (Elsevier, Amsterdam, 2008).
29. T. Jonsson, N. Folkeson, M. Halvarsson, J.-E. Svensson and L.-G. Johansso, *Oxidation of Metals* **81**, 575 (2014).
30. I. Gurrappa, S. Weinbruch, D. Naumenko and W. J. Quadakkers, *Materials and Corrosion* **51**, 224 (2000).